Magnetic Properties

International Edition: DOI: 10.1002/anie.201503636
German Edition: DOI: 10.1002/ange.201503636

# Influence of Guest Exchange on the Magnetization Dynamics of Dilanthanide Single-Molecule-Magnet Nodes within a Metal–Organic Framework**

*Xuejing Zhang, Veacheslav Vieru, Xiaowen Feng, Jun-Liang Liu, Zhenjie Zhang, Bo Na, Wei Shi,* Bing-Wu Wang, Annie K. Powell, Liviu F. Chibotaru,* Song Gao,* Peng Cheng, and Jeffrey R. Long**

**Abstract:** *Multitopic organic linkers can provide a means to organize metal cluster nodes in a regular three-dimensional array. Herein, we show that isonicotinic acid N-oxide (HINO) serves as the linker in the formation of a metal–organic framework featuring $Dy_2$ single-molecule magnets as nodes. Importantly, guest solvent exchange induces a reversible single-crystal to single-crystal transformation between the phases $Dy_2(INO)_4(NO_3)_2{\cdot}2\,solvent$ (solvent = DMF ($Dy_2$-DMF), $CH_3CN$ ($Dy_2$-$CH_3CN$)), thereby switching the effective magnetic relaxation barrier (determined by ac magnetic susceptibility measurements) between a negligible value for $Dy_2$-DMF and 76 $cm^{-1}$ for $Dy_2$-$CH_3CN$. Ab initio calculations indicate that this difference arises not from a significant change in the intrinsic relaxation barrier of the $Dy_2$ nodes, but rather from a slowing of the relaxation rate of incoherent quantum tunneling of the magnetization by two orders of magnitude.*

Single-molecule magnets (SMMs) are discrete molecules exhibiting magnet-like behavior and have attracted considerable attention for potential applications in high-density information storage and nanoscale electronics.[1] Lanthanide ions provide many of the best examples of SMMs, owing to the significant magnetic anisotropy originating from strong spin-orbit coupling and crystal-field effects, which can lead to large spin reversal energy barriers.[2] However, the factors influencing the magnetization dynamics for lanthanide-based SMMs are still obscured by the complicated magnetic nature of lanthanide ions, including the spin-orbit coupling, high magnetic anisotropy, weak magnetic exchange interactions, and multiple relaxation pathways. The main factor that governs the intrinsic relaxation barrier for such species is considered to be symmetry-related single-ion anisotropy.[2c,3] Other factors, such as hyperfine couplings, dipolar spin–spin interactions, and transverse internal fields, could also lower the effective relaxation energy barrier by introducing fast quantum tunneling of the magnetization.[1b,4] The hyperfine couplings can be effectively tuned by utilizing isotopically pure or enriched lanthanide sources,[5] whereas the other two factors, spin–spin interactions and transverse internal fields, can be suppressed by magnetic dilution[5,6] or strong exchange interactions between lanthanide ions.[7] To date, it is often still quite challenging to prepare isotopically enriched or magnetically dilute samples or, in particular, to introduce strong magnetic exchange coupling in most lanthanide systems.[5–7] In this context, a regular platform that can provide fine tuning of SMM behavior is of great interest to the field.

Metal–organic frameworks (MOFs) constructed from inorganic nodes and organic linkers are a promising class of functional molecule-based materials because their highly porous structures can accommodate a wide variety of differ-

[*] X. Zhang, Dr. Z. Zhang, Dr. B. Na, Prof. Dr. W. Shi, Prof. Dr. P. Cheng
Department of Chemistry
Key Laboratory of Advanced Energy Materials Chemistry (MOE)
State Key Laboratory of Elemento-Organic Chemistry
Collaborative Innovation Center of Chemical Science and Engineering (Tianjin), Nankai University
Tianjin 300071 (P. R. China)
E-mail: shiwei@nankai.edu.cn

Prof. Dr. B.-W. Wang, Prof. Dr. S. Gao
Beijing National Laboratory of Molecular Science
State Key Laboratory of Rare Earth Materials Chemistry and Applications, College of Chemistry and Molecular Engineering
Peking University, Beijing 100871 (P. R. China)
E-mail: gaosong@pku.edu.cn

Prof. Dr. A. K. Powell
Institute of Inorganic Chemistry, Karlsruhe Institute of Technology
Engesserstrasse 15, 76131 Karlsruhe (Germany)

V. Vieru, Prof. Dr. L. F. Chibotaru
Theory of Nanomaterials Group and INPAC—Institute of Nanoscale Physics and Chemistry, Katholieke Universiteit Leuven
Celestijnenlaan 200F, 3001 Heverlee (Belgium)
E-mail: Liviu.Chibotaru@chem.kuleuven.be

X. Feng, J.-L. Liu, Prof. Dr. J. R. Long
Department of Chemistry, University of California, Berkeley
Berkeley, CA 94720 (USA)
E-mail: jrlong@berkeley.edu

[**] This work was supported by the "973" program (grant number 2012CB821702), the NSFC (grant numbers 21331003, 21373115, and 91422302) and the MOE (grant numbers NCET-13-0305 and IRT-13R30). Research at UC Berkeley was carried out within the Nanoporous Materials Genome Center, which is supported by the U.S. Department of Energy, Office of Basic Energy Sciences, Division of Chemical Sciences, Geosciences, and Biosciences under award DE-FG02-12ER16362. We thank very much Dr. Chen Gao from Peking University for the help with PPMS measurement. We also thank the reviewers for their valuable comments which have improved the manuscript.

Supporting information for this article is available on the WWW under http://dx.doi.org/10.1002/anie.201503636.

  

ent guest molecules. MOFs have shown great potential for a number of applications, including gas storage and separations,[8,9] chemical sensing,[10] and catalysis.[11] A current synthetic challenge, however, is to create porous MOFs in which SMMs serve as the nodes, thereby providing a means of tuning the magnetization dynamics through the influence of different guest molecules within the pores. In principle, different sizes, shapes, and hydrogen-bonding capabilities of the guest molecules could drastically influence the SMM behavior, as has been demonstrated for example by supramolecular effects within a series of molecular species of the type $Ln^{III}$-DOTA ($H_4$DOTA = 1,4,7,10-tetraazacyclododecane-*N*,*N*′,*N*″,*N*‴-tetraacetic acid).[12]

Herein, we demonstrate how the magnetization dynamics of SMM nodes in a lanthanide-based MOF can be tuned through guest exchange.[6d,13,14] Specifically, a new MOF system containing a binuclear $Dy^{III}$ node, namely $Dy_2(INO)_4(NO_3)_2\cdot 2$solvent (HINO = isonicotinic acid *N*-oxide; solvent = DMF ($Dy_2$-DMF), $CH_3CN$ ($Dy_2$-$CH_3CN$)) and $Dy_2(INO)_4(NO_3)_2$ ($Dy_2$-A) without solvent, is introduced and investigated for guest-dependent magnetic properties. As a result of the porous nature of the structure, exchange of the guest molecules can be achieved through a single-crystal to single-crystal transformation, leading to major changes in the magnetic relaxation behavior. As demonstrated using ab initio calculations, this effect is a result of the high sensitivity of the crystal field of the $Dy^{III}$ ions to modifications in their environment.

The metal–organic framework $Dy_2$-DMF was synthesized by the solvothermal reaction of $Dy(NO_3)_3\cdot 6H_2O$ with HINO in DMF. In view of its porous structure and thermal stability (see Figure S1 in the Supporting Information), a solvent exchange reaction was performed (Scheme 1). The isomorphic phase $Dy_2$-$CH_3CN$ was obtained by soaking $Dy_2$-DMF in six sequential aliquots of acetonitrile at room temperature. The exchanged solvent molecules in $Dy_2$-$CH_3CN$ could be readily resolved by single-crystal X-ray diffraction analysis, and complete exchange was further confirmed by elemental analysis and thermogravimetric analysis. Significantly, this single-crystal to single-crystal transformation is fully reversible, as determined by both single-crystal and powder X-ray diffraction analyses (see Table S1 and Figure S2 in the Supporting Information). Moreover, the evacuated framework ($Dy_2$-A) without any guest solvent was successfully prepared and fully characterized (Tables S1, Figure S1, S2).

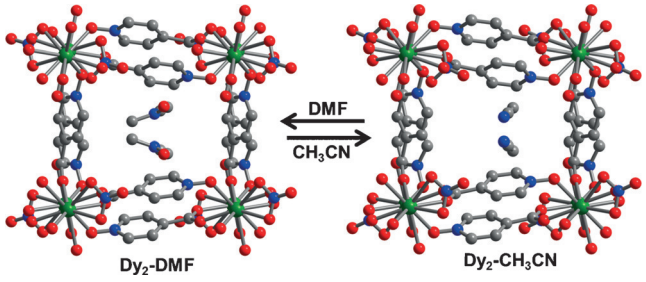


***Scheme 1.*** Synthetic route and single-crystal to single-crystal transformation between $Dy_2$-DMF and $Dy_2$-$CH_3CN$. Atom colors: Dy = green, O = red, N = blue, C = gray. H atoms have been omitted for clarity.

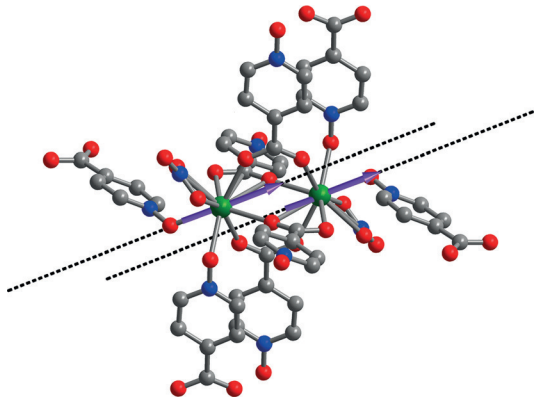

***Figure 1.*** The coordination environment of the $Dy^{III}$ centers within the binuclear $Dy_2$ units of $Dy_2$-DMF. The dashed lines show the main anisotropy axes for each metal and the arrows indicate the local magnetic moments in the ground exchange doublet state.

The crystal structure of the parent phase $Dy_2$-DMF consists of binuclear $Dy_2$ units connected within a porous three-dimensional network (Scheme 1 and Figure 1). The structure features just one crystallographically independent $Dy^{III}$ center, situated within a monocapped square antiprism coordination environment (approximately $C_{4v}$ symmetry) comprising two O atoms from a $NO_3^-$ ion and seven O atoms from six different $INO^-$ linkers. Two $\mu_2$-O atoms from carboxylate groups and two $\mu_{1,3}$-carboxylate groups bridge the two $Dy^{III}$ centers to form the binuclear units, which reside upon crystallographic inversion centers.

The main distinctions between the crystal structures of $Dy_2$-DMF and $Dy_2$-$CH_3CN$ arise from the differing solvent molecules residing within the pores and how they interact with the surrounding framework (Figure S3). These effects lead to subtle differences in the structures of the $Dy_2$ units: the Dy···Dy separations are 4.0483(3) and 4.0090(2) Å, the Dy–O distances range from 2.312(2)–2.737(3) Å and 2.323(2)–2.667(2) Å, and the Dy-O-Dy angles are 106.29(8)° and 106.73(8)° for $Dy_2$-DMF and $Dy_2$-$CH_3CN$, respectively. Variations in the C–H···O(N) hydrogen-bonding interactions as a result of the different guest molecules are responsible for the minor differences of the coordination environments of the $Dy^{III}$ centers (Table S2). It is noted that an almost identical structural form of $Dy_2$-A with $Dy_2$-MeCN but not with $Dy_2$-DMF was found by the comparison of the crystal structures of the three frameworks. We also note that the $Dy_2$···$Dy_2$ separation between the midpoints of neighboring $Dy_2$ units are all greater than 10 Å, suggesting an absence of significant magnetic exchange interactions between binuclear units.

Direct current (dc) magnetic susceptibility data were collected for the three MOFs in the temperature range 2–300 K under an applied field of 1 kOe (Figure 2 and Figure S4). The $\chi_M T$ values (where $\chi_M$ is the molar magnetic susceptibility) at 300 K are 28.12, 28.32, and 28.07 $cm^3 K mol^{-1}$ for $Dy_2$-DMF, $Dy_2$-$CH_3CN$, and $Dy_2$-A, respectively, which are close to the expected value of 28.34 $cm^3 K mol^{-1}$ for two non-interacting $Dy^{III}$ centers ($^6H_{15/2}$, $S = 5/2$, $L = 5$, $J = 15/2$,

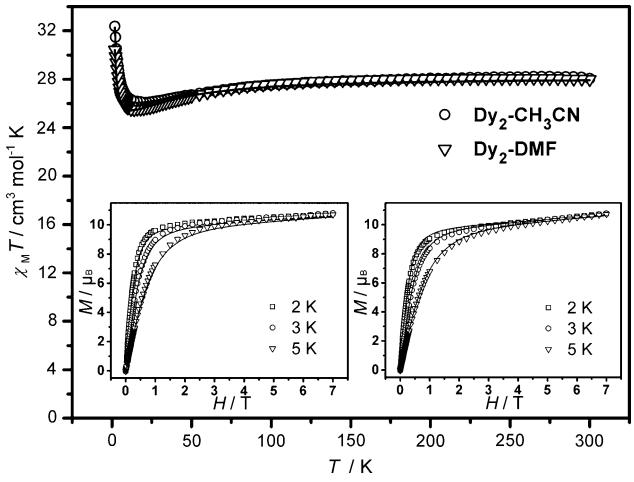


***Figure 2.*** Temperature dependence of the $\chi_M T$ value at 1000 Oe for $Dy_2$-DMF (▽) and $Dy_2$-$CH_3CN$ (○). Inset: Plots of magnetization ($M$) versus applied field ($H$) at 2, 3, and 5 K for $Dy_2$-$CH_3CN$ (left) and $Dy_2$-DMF (right). The solid lines correspond to calculated fits to the data.

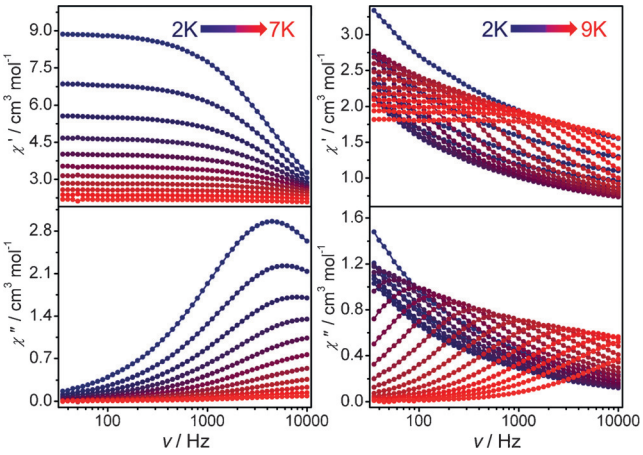


***Figure 3.*** Frequency dependence of in-phase ($\chi'$) and out-of-phase ($\chi''$) ac susceptibilities under zero dc field at indicated temperatures for $Dy_2$-DMF (left) and $Dy_2$-$CH_3CN$ (right).

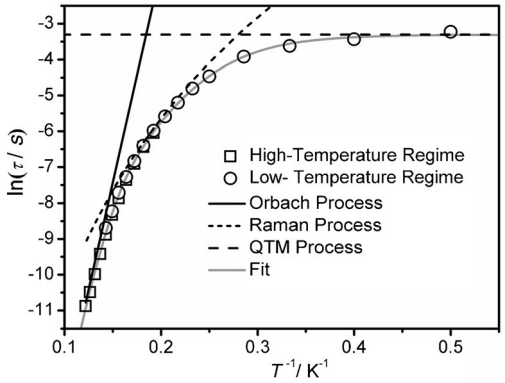


***Figure 4.*** A plot of $\ln(\tau/s)$ versus $T^{-1}$ for $Dy_2$-$CH_3CN$. Data in the high-temperature regime were obtained using a PPMS instrument, and data in the low-temperature regime were measured using a SQUID-VSM instrument. All data were collected under zero dc field. QTM = quantum tunneling of magnetization.

$g = 4/3$). Upon lowering the temperature, the $\chi_M T$ value decreases gradually to minima of 25.53, 26.50, and 25.71 $cm^3 K mol^{-1}$ at 12, 20, and 12 K, before increasing abruptly to reach values of 30.42, 33.94, and 31.66 $cm^3 K mol^{-1}$ at 2 K for $Dy_2$-DMF, $Dy_2$-$CH_3CN$, and $Dy_2$-A, respectively. The increases in $\chi_M T$ at very low temperature suggest that ferromagnetic coupling starts to dominate the magnetic behavior for the ground state of each material. At 2 K, the magnetization increases steeply upon increasing the magnetic field strength, reaching saturation values of 10.76, 10.78, and 10.54 $\mu_B$ for $Dy_2$-DMF, $Dy_2$-$CH_3CN$, and $Dy_2$-A, respectively, indicating well-separated excited states. This is confirmed by ab initio calculations (see below).

The isostructural nature of the three frameworks, and especially the very similar core structures of the binuclear nodes, might be anticipated to give rise to similar magnetization dynamics at low temperature. However, ac magnetic susceptibility data collected under zero applied dc field reveal significant differences in the observed relaxation behavior (Figure 3 and Figures S5–S9), indicating the dominance of differing relaxation mechanisms depending on the guest molecules present within the pores. For $Dy_2$-DMF, the peaks in the out-of-phase ac susceptibility only appear at very high frequencies of near 10 kHz. The correlation between the relaxation time ($\tau$) and temperature ($T$) can be obtained from a plot of $\ln(\tau)$ versus $\ln(T)$ to give an $n$ value of 1.7 ($n$ is the parameter that represents the relation between relaxation time and temperature in the equation $\tau = T^{-n}$), indicating that relaxation occurs mainly by a direct process (Figure S10). In contrast, for $Dy_2$-$CH_3CN$ slow magnetic relaxation was observed for a wide range of frequencies and temperatures. To distinguish between glassiness and superparamagnetism, the parameter $\phi$, derived from the equation $\phi = (\Delta T_p/T_p)/\Delta(\log \nu)$, was calculated ($T_p$ is the peak temperature of the in-phase ac susceptibilities).[15] The calculated value of $\phi = 0.18$ lies within the range 0.1–0.3, as expected for superparamagnetic behavior. To extract relaxation times, ac susceptibility data can be fitted with a generalized Debye model, as shown in Cole–Cole plots (Figure S7–S9, Tables S3, S4).[16] The resulting temperature dependence of the relaxation time is shown in Figure 4. Spin-lattice relaxation processes, such as Raman or quantum tunneling processes, can coexist with Orbach (or thermally-activated) relaxation, but dominate in a different temperature range. At high temperatures, an Orbach process is mainly responsible for the relaxation, whereas at low temperatures gradual transitions are observed as a result of non-Orbach relaxation. A fit employing Equation (1) (where $\tau_{QTM}$ is the quantum tunneling of magnetization relaxation time, $C$ is the coefficient of Raman process, $U_{eff}$ is the energy barrier to magnetization reversal, and $k_B$ is the Boltzmann constant) gives good agreement with the data over the entire temperature range with parameters of $\tau_{QTM}^{-1} = 26.8\ s^{-1}$, $C = 0.0057\ s^{-1} K^{-6.69}$, $n = 6.69$, $\tau_0 = 3.24 \times 10^{-11}$ s, and $U_{eff} = 76\ cm^{-1}$ (110 K). For $Dy_2$-A, the magnetization dynamics are very close to those of $Dy_2$-$CH_3CN$ because of the almost identical structural form of $Dy_2$-A with $Dy_2$-MeCN (Figures S5, S6, S9, S11 and Table S5).

From the analysis of the ac data, a fit employing Equation (1) also gives good agreement with the data over the entire temperature range (Figure S11) with parameters of $\tau_{QTM}^{-1} = 26.3\ s^{-1}$, $C = 0.0476\ s^{-1}K^{-5.71}$, $n = 5.71$, $\tau_0 = 1.81 \times 10^{-11}$ s, and $U_{eff} = 67\ cm^{-1}$ (97 K).

$$\tau^{-1} = \tau_{QTM}^{-1} + CT^n + \tau_0^{-1}\exp(-U_{eff}/k_B T) \quad (1)$$

To elucidate the differences in magnetization relaxation dynamics between $Dy_2$-DMF and $Dy_2$-$CH_3CN$ (or $Dy_2$-A), ab initio calculations were performed at the CASSCF/SO-RASSI/SINGLE_ANISO level using the Molcas 7.8 program (Tables S6–S9, Figure S14 and S15).[17] The levels for the low-lying spectra associated with the $Dy^{III}$ centers are listed in Table S7, and the *g* tensors of the lowest-lying Kramers doublets are provided in Table S8. From this data, the first-excited Kramers doublet is evident at 60, 66, and 53 $cm^{-1}$ for $Dy_2$-$CH_3CN$, $Dy_2$-A, and $Dy_2$-DMF, respectively. Both computational approximations, small fragment with a bigger basis set and larger fragment with a smaller basis set, predict that the ground Kramers doublet is less axial in the case of the DMF analogue than for the acetonitrile compound or for the evacuated framework (Table S8). Owing to the presence of an inversion center in the $Dy_2$ unit of both MOFs, the main anisotropy axes of the $Dy^{III}$ centers are parallel to each other, as shown in Figure 1.

The dipolar interaction between the $Dy^{III}$ centers within a binuclear unit was calculated on the basis of ab initio results, while the magnetic exchange interaction was taken into account within the Lines model[17a,18] using the POLY_ANISO program. The Lines exchange parameters were determined by fitting the experimental magnetic susceptibility data (Figure 2 and Figure S4). As shown in Table S9, the dipolar interaction is stronger than the exchange interaction and stabilizes the parallel alignment of the local magnetic moments of the $Dy^{III}$ centers in the ground exchange doublet (Figure 1). The tunneling gap ($\Delta_{tun}$) for the Dy sites induced by the dipolar applied magnetic field ($H_{dip}$) from the surrounding metal ions, $\Delta_{tun} = 1/2\, g_{x,y}\mu_B H_{dip}$ ($\mu_B$ is the Bohr magneton), is estimated as approximately $10^{-3}\ cm^{-1}$ for $Dy_2$-$CH_3CN$ or $Dy_2$-A and approximately $10^{-2}\ cm^{-1}$ for $Dy_2$-DMF. These estimates correspond to a transverse field of 100 mT for $Dy_2$-$CH_3CN$ or $Dy_2$-A and 90 mT for $Dy_2$-DMF, arising from one nearest Dy neighbor. As the relaxation rate of incoherent quantum tunneling is proportional to $\Delta_{tun}^2$, it is clear that it will be circa $10^2$ times slower in $Dy_2$-$CH_3CN$ or $Dy_2$-A than in $Dy_2$-DMF, explaining why the former two compounds are good SMMs, while the latter is not.[1d] The experimentally extracted barriers of 76 and 67 $cm^{-1}$ for $Dy_2$-$CH_3CN$ and $Dy_2$-A can be firmly attributed to the relaxation via the first-excited Kramers doublet of the $Dy^{III}$ centers. Indeed, the calculated first Kramers doublets for the $Dy^{III}$ centers in $Dy_2$-$CH_3CN$ is located at 60 $cm^{-1}$ (see Table S7), and that of $Dy_2$-A lies at 66 $cm^{-1}$, in reasonable agreement with the experimental results. The foregoing results clearly reveal the origin of the magnetization dynamics: a) the similar energy barriers are mainly from the single-ion anistropy of the $Dy^{III}$ centers because of the similar coordination environments; b) the subtle differences caused by either the guest molecules or no guest molecule lead to different dipole–dipole interactions which tune the relaxation rate of incoherent quantum tunneling to give drastically different effective relaxation barriers.

Additionally, considering that the single-ion anisotropy contributions from the two $Dy^{III}$ centers in the bimetallic units are symmetry related, the continuous symmetry measure (CSM) method was employed to evaluate the deviation from an ideal monocapped square antiprismatic coordination geometry.[19] Herein, the larger the calculated CSAPR-9 parameter, the greater the deviation from an ideal $C_{4v}$ symmetry. The calculated CSAPR-9 parameters are 2.011, 1.727, and 1.879 for $Dy_2$-DMF, $Dy_2$-$CH_3CN$, and $Dy_2$-A, respectively, indicating that there is relatively little geometric difference between the binuclear units in all the three structures. This is further consistent with the results of the ab initio calculations of the similar energy gaps between the ground and the first excited states for the $Dy^{III}$ centers in all compounds. Thus, the different solvent molecules or no solvent molecule within the pores of the MOF play an important role in influencing the dipole–dipole interactions, in accordance with the very different magnetic dynamics observed. Accordingly, the ab initio calculations based on the single-crystal structures afford substantially different values for the dipolar coupling of 2.11 $cm^{-1}$ for $Dy_2$-DMF, 1.81 $cm^{-1}$ for $Dy_2$-$CH_3CN$, and 1.81 $cm^{-1}$ for $Dy_2$-A. To our knowledge, this is the first example in which guest molecules are employed to adjust the dipole–dipole interactions and thereby tune the relaxation rates arising from incoherent quantum tunneling of the magnetization.

In summary, exchange of the guest molecules within the pores of a new lanthanide-based MOF featuring binuclear $Dy_2^{III}$ single-molecule magnets as nodes has been demonstrated to impart major changes in the magnetization relaxation dynamics. Guest exchange reactions interconverting the two frameworks from single-crystal to single-crystal were successfully performed using DMF and acetonitrile. Magnetic susceptibility measurements and ab initio calculations have shown that the subtle structural changes associated with guest solvent exchange can lead to drastic improvements in SMM behavior. This work not only illustrates a chemical means of combining SMMs and MOFs in molecule-based materials, but also provides a powerful new platform for tuning SMM behavior.

**Keywords:** ab initio calculations · host–guest systems · lanthanides · metal–organic frameworks · single-molecule magnets

**How to cite:** *Angew. Chem. Int. Ed.* **2015**, *54*, 9861–9865
*Angew. Chem.* **2015**, *127*, 9999–10003

[1] a) M. N. Leuenberger, D. Loss, *Nat. Chem.* **2001**, *410*, 789–793; b) D. Gatteschi, R. Sessoli, *Angew. Chem. Int. Ed.* **2003**, *42*, 268–297; *Angew. Chem.* **2003**, *115*, 278–309; c) S. Hill, R. S. Edwards, N. Aliaga-Alcalde, G. Christou, *Science* **2003**, *302*, 1015–1018; d) D. Gatteschi, R. Sessoli, J. Villain, *Molecular Nanomagnets*, Oxford University Press, Oxford, **2006**; e) L. Bogani, W. Wernsdorfer, *Nat. Mater.* **2008**, *7*, 179–186; f) P. Jarillo-Herrero, *Science* **2010**, *328*, 1362–1363; g) M. Mannini, F. Pineider, C.

  

Danieli, F. Totti, L. Sorace, P. Sainctavit, M.-A. Arrio, E. Otero, L. Joly, J. C. Cezar, A. Cornia, R. Sessoli, *Nature* **2010**, *468*, 417 – 421; h) S. Thiele, F. Balestro, R. Ballou, S. Klyatskaya, M. Ruben, W. Wernsdorfer, *Science* **2014**, *344*, 1135 – 1138.

[2] a) R. Sessoli, A. K. Powell, *Coord. Chem. Rev.* **2009**, *253*, 2328 – 2341; b) B. W. Wang, S. D. Jiang, X. T. Wang, S. Gao, *Sci. China Ser. B* **2009**, *11*, 1739 – 1758; c) J. D. Rinehart, J. R. Long, *Chem. Sci.* **2011**, *2*, 2078 – 2085; d) L. Sorace, C. Benelli, D. Gatteschi, *Chem. Soc. Rev.* **2011**, *40*, 3092 – 3104; e) D. N. Woodruff, R. E. P. Winpenny, R. A. Layfield, *Chem. Rev.* **2013**, *113*, 5110 – 5148.

[3] a) N. Ishikawa, M. Sugita, T. Ishikawa, S.-y. Koshihara, Y. Kaizu, *J. Am. Chem. Soc.* **2003**, *125*, 8694 – 8695; b) M. A. AlDamen, J. M. Clemente-Juan, E. Coronado, C. Martí-Gastaldo, A. Gaita-Ariño, *J. Am. Chem. Soc.* **2008**, *130*, 8874 – 8875; c) S. D. Jiang, B. W. Wang, H. L. Sun, Z. M. Wang, S. Gao, *J. Am. Chem. Soc.* **2011**, *133*, 4730 – 4733; d) C. R. Ganivet, B. Ballesteros, G. de La Torre, J. M. Clemente-Juan, E. Coronado, T. Torres, *Chem. Eur. J.* **2013**, *19*, 1457 – 1465; e) J.-L. Liu, Y.-C. Chen, Y.-Z. Zheng, W.-Q. Lin, L. Ungur, W. Wernsdorfer, L. F. Chibotaru, M.-L. Tong, *Chem. Sci.* **2013**, *4*, 3310 – 3316.

[4] a) N. Ishikawa, M. Sugita, W. Wernsdorfer, *J. Am. Chem. Soc.* **2005**, *127*, 3650 – 3651; b) N. Ishikawa, M. Sugita, R. Clérac, W. Wernsdorfer, *Angew. Chem. Int. Ed.* **2005**, *44*, 2931 – 2935; *Angew. Chem.* **2005**, *117*, 2991 – 2995.

[5] F. Pointillart, K. Bernot, S. Golhen, B. L. Guennic, T. Guizouarn, L. Ouahab, O. Cador, *Angew. Chem. Int. Ed.* **2015**, *54*, 1504 – 1507; *Angew. Chem.* **2015**, *127*, 1524 – 1527.

[6] a) S. D. Jiang, B. W. Wang, G. Su, Z. M. Wang, S. Gao, *Angew. Chem. Int. Ed.* **2010**, *49*, 7448 – 7451; *Angew. Chem.* **2010**, *122*, 7610 – 7613; b) F. Habib, P. H. Lin, J. Long, I. Korobkov, W. Wernsdorfer, M. Murugesu, *J. Am. Chem. Soc.* **2011**, *133*, 8830 – 8833; c) K. R. Meihaus, J. R. Long, *J. Am. Chem. Soc.* **2013**, *135*, 17952 – 17957; d) B. Na, X.-J. Zhang, W. Shi, Y.-Q. Zhang, B.-W. Wang, C. Gao, S. Gao, P. Cheng, *Chem. Eur. J.* **2014**, *20*, 15975 – 15980.

[7] a) J. D. Rinehart, M. Fang, W. J. Evans, J. R. Long, *Nat. Chem.* **2011**, *3*, 538 – 542; b) Y.-N. Guo, G.-F. Xu, W. Wernsdorfer, L. Ungur, Y. Guo, J. Tang, H.-J. Zhang, L. F. Chibotaru, A. K. Powell, *J. Am. Chem. Soc.* **2011**, *133*, 11948 – 11951; c) J. D. Rinehart, M. Fang, W. J. Evans, J. R. Long, *J. Am. Chem. Soc.* **2011**, *133*, 14236 – 14239; d) S. Demir, J. Zadrozny, M. Nippe, J. R. Long, *J. Am. Chem. Soc.* **2012**, *134*, 18546 – 18549.

[8] a) E. D. Bloch, W. L. Queen, R. Krishna, J. M. Zadrozny, C. M. Brown, J. R. Long, *Science* **2012**, *335*, 1606 – 1610; b) Z. R. Herm, B. M. Wiers, J. A. Mason, J. M. van Baten, M. R. Hudson, P. Zajdel, C. M. Brown, N. Masciocchi, R. Krishna, J. R. Long, *Science* **2013**, *340*, 960 – 964.

[9] T. A. Makal, J.-R. Li, W. Lu, H.-C. Zhou, *Chem. Soc. Rev.* **2012**, *41*, 7761 – 7779.

[10] a) J. Rocha, L. D. Carlos, F. A. Almeida Paz, D. Ananias, *Chem. Soc. Rev.* **2011**, *40*, 926 – 940; b) J. Heine, K. Müller-Buschbaum, *Chem. Soc. Rev.* **2013**, *42*, 9232 – 9242.

[11] A. Corma, H. Garcia, F. X. L. Xamena, *Chem. Rev.* **2010**, *110*, 4606 – 4655.

[12] a) G. Cucinotta, M. Perfetti, J. Luzon, M. Etienne, P.-E. Car, A. Caneschi, G. Calvez, K. Bernot, R. Sessoli, *Angew. Chem. Int. Ed.* **2012**, *51*, 1606 – 1610; *Angew. Chem.* **2012**, *124*, 1638 – 1642; b) M.-E. Boulon, G. Cucinotta, J. Luzon, C. Degl'Innocenti, M. Perfetti, K. Bernot, G. Calvez, A. Caneschi, R. Sessoli, *Angew. Chem. Int. Ed.* **2013**, *52*, 350 – 354; *Angew. Chem.* **2013**, *125*, 368 – 372.

[13] W. Shi, K. Liu, P. Cheng, *Struct. Bonding (Berlin)* **2015**, *163*, 231 – 263.

[14] a) Y. Wang, W. Shi, H. Li, Y. Song, L. Fang, Y. Lan, A. K. Powell, W. Wernsdorfer, L. Ungur, L. F. Chibotaru, M. Shen, P. Cheng, *Chem. Sci.* **2012**, *3*, 3366 – 3370; b) T. Han, W. Shi, X. P. Zhang, L. L. Li, P. Cheng, *Inorg. Chem.* **2012**, *51*, 13009 – 13016; c) T. Han, W. Shi, Z. Niu, B. Na, P. Cheng, *Chem. Eur. J.* **2013**, *19*, 994 – 1001; d) S. Zhang, W. Shi, L. Li, E. Duan, P. Cheng, *Inorg. Chem.* **2014**, *53*, 10340 – 10346; e) K. Liu, W. Shi, P. Cheng, *Coord. Chem. Rev.* **2015**, *289 – 290*, 74 – 122.

[15] J. A. Mydosh, *Spin Glasses: An Experimental Introduction*, Taylor & Francis, London, **1993**.

[16] M. Hagiwara, *J. Magn. Magn. Mater.* **1998**, *177 – 181*, 89 – 90.

[17] a) L. F. Chibotaru, L. Ungur, C. Aronica, H. Elmoll, G. Pilet, D. Luneau, *J. Am. Chem. Soc.* **2008**, *130*, 12445 – 12455; b) F. Aquilante, L. De Vico, N. Ferre, G. Ghigo, P.-A. Malmqvist, P. Neogrady, T. B. Pedersen, M. Pitonak, M. Reiher, B. O. Roos, L. Serrano-Andres, M. Urban, V. Veryazov, R. Lindh, *J. Comput. Chem.* **2010**, *31*, 224 – 247; c) L. F. Chibotaru, L. Ungur, *J. Chem. Phys.* **2012**, *137*, 064112; d) http://molcas.org/documentation/manual.

[18] M. E. Lines, *J. Chem. Phys.* **1971**, *55*, 2977 – 2984.

[19] a) H. Zabrodsky, S. Peleg, D. Avnir, *J. Am. Chem. Soc.* **1992**, *114*, 7843 – 7851; b) M. Pinsky, D. Avnir, *Inorg. Chem.* **1998**, *37*, 5575 – 5582.

Received: April 21, 2015
Revised: May 20, 2015
Published online: June 26, 2015

  